Engineering and Technology Journal
Journal homepage: https://etj.uotechnology.edu.iq

Electrophoretic Deposition Used to Prepare And Analyze The Microstructure of Chitosan/Hydroxyapatite Nano-Composites

Israa Z. Ahmed*, Hussein A. Jaber, Shaymaa M. Salih

Materials Engineering Dept., University of Technology-Iraq, Alsina'a Street, 10066 Baghdad, Iraq.
*Corresponding author Email: mae.19.22@grad.uotechnology.edu.iq

HIGHLIGHTS

- Pulsed EPD improved the coating layer by degreasing the bubbles and cracks.
- Using an FTIR test, major chemical bonds were found to the HAP and CS.
- Little frequency in the PEPD causes degreasing distortion in the coating layer.

ARTICLE INFO

Handling editor: Jawad K. Oleiwi

Keywords:
Electrophoretic deposition; Nano-composite; Chitosan; Nano- hydroxyapatite.

ABSTRACT

This research studies the coating layer properties from chitosan and nano – hydroxyapatite made by pulsed electrophoretic deposition (PEPD) for biomedical applications. The 316L SS alloys were coated with hydroxyapatite in different solutions in 100 mL of suspension at a 30 V continuous voltage. To characterize the deposited coatings, X-ray diffraction spectroscopy (XRD), Fourier transform infrared (FTIR), Contact Angle, scanning electron microscopy (SEM), energy dispersive x-ray analysis (EDX),Yield deposition and Optical microscopy structural (OM) was used for coating layer, in addition to being calculated Zeta potential for suspensions. The aim of this study is to show that using the Pulsed EPD method at room temperature, a simple and low-cost solution for in situ synthesis of Nano -HAp within a chitosan matrix for biomedical applications can be demonstrated.

1. Introduction

Biomaterials are synthetic or natural materials that are used in biological settings to direct, supplement, or replace the roles of living tissues in the human body. Metals, polymers, ceramics, and composites are among the materials that can be used to create nanoparticles. Metals stand out among these different materials for the production of biomaterials because of their high mechanical properties, low cost, and ease of manufacture [1]. Stainless steel (SS) is the first alloy to be successfully used as biomedical implants, with more than 12 percent chromium for excellent corrosion resistance. Due to their good ductility, high yield, and young modulus, as well as the ability to replace hard tissue function, they are suitable for load bearing [2].316L SS are identical to those of human bone, and its cost is very low as compared to other implants, in addition, it has excellent physiochemical corrosion resistance, chemical resilience, formability, and power [3]. Hydroxyapatite (HAp) is a calcium phosphate ceramic substance that resembles the inorganic sections of human bone and teeth in morphology and composition. Because of its excellent osteo-conductivity, biocompatibility, and bioactivity, HAp was widely used in biomedical applications. Commercially available HAp comes from either a natural or synthetic source [4].Chitosan is one of the most commonly used natural biopolymers for a wide range of biomedical applications due to its biocompatibility, biodegradability, and antibacterial activity, and is generally regarded as a healthy material, for particles in suspension, it can be used as a dispersant, binder, and surface charge agent, solubility, crystallinity, biodegradability, viscosity, and biocompatibility are all important physical, chemical, and biological properties of chitosan [5]. Chemical modifications can tailor chitosan's solubility, biocompatibility, hydrophobicity, and many other properties, allowing it to be used in a wide range of applications. Electrophoretic deposition (EPD) is the most widely used technique for producing chitosan coatings, since it allows the control of deposition parameters to obtain films with specific properties on substrates with complex geometries, besides the possibility of obtaining coatings at room temperature. The goal of this work is to use pulsed EPD to investigate the effects of HAp-CS coating on 316L SS to increase biocompatibility for biomedical applications [6].

2. Experimental Materials and Methods

2.1 Suspensions Preparation and Materials Used

The important step in the experimental procedure of pulsed electrophoretic deposition (PEPD) is to prepare the aqueous suspensions as follows: dissolve 0.5g/L of chitosan using 1% acetic acid in a glass beaker 100 ml [7, 8]. After that, the

http://doi.org/10.30684/etj.v39i11.2181
Received 24 May 2021; Accepted 19 August 2021; Available online 25 November 2021
2412-0758/

mixtures of ethanol 79% and 20% deionized water were added to the glass beaker. The mixture was magnetically stirred for 15 min and then Nano-powder varying the concentration (from 0.15 g/100L to 0.6 g/100L HAp) was added. After that, the suspension was covered with Para- film to prevent evaporation. Both suspensions were magnetically stirred for 20 minutes to break down particle agglomeration and achieve homogeneous dispersion and increased particle stability. Finally, the mixture was solicited for 20 minutes to break up fragile agglomerates and give the particles in the suspension a homogenized dispersion. The pH meter with acetic acid was used to adjust the range of pH values at (4.5 ± 0.5) of suspensions. The materials used in this study to make a HAp/CS composite coating, along with their purity and origin: Hydroxyapatite (HAp) Nano powder have formula $Ca_5(OH)(PO_4)_3$ (Hualanchem. Co. China) with primary particles size of 40 nm and purity (96%), melting point 1100 C and molecular weight 502.31) on 316L stainless steel, it was used to deposit a coating sheet. Chitosan (CS) has the formula $(C_8H_{13}O_5N)_n$ A binder with HAp powder had a purity of 99.8% (Medium molecular weight with a degree of deacetylation of around85%, soluble in 1% acetic acid, manufactured in China). The solvent of ethanol absolute with purity (99.9%) has formula (C_2H_5OH), (made in Spain) was used as a medium to coatings. In this analysis, acetic acid with the formula CH3COOH9 (made in India) and purity (99.7%) was used to dissolve Hydroxyapatite.

2.2 Preparation of Substrate

Stainless steel 316L electrode plates (15* 15 *1) mm were coated with 600 and 1200 silicon carbide paper and washed in distilled water before being ultrasonically cleaned with 50 ml ethanol and 50 ml acetone for 15 minutes and dried immediately before the electrophoretic coating operation.

2.3 Pulsed Electrophoretic Technique

The EPD cell used in this study consists of a beaker (100 ml), two electrodes immersed in the suspension, a power supply connected in a series arrangement to the cathode (negative electrode) and the anode (positive electrode) as well as jack to raise the suspension towards the electrodes and lower it after finishing the coating process, Pulsed device (Handmade). The system diagram is shown in Figure 1. 316L stainless steel alloys were used as counter electrodes (anode) and active electrodes in pulsed electrophoretic deposition (cathode). The cathodic and anodic electrodes were washed in ethanol and dry before deposition, which was accomplished by drenching the electrodes in a 100 ml beaker filled with solution. In the EPD cell, the distance between electrodes was held constant at 10mm, and only 1.8 cm^2 of the substrate was exposed to deposition. By adjusting the deposition time (from 10 to 20 minutes) and applying constant voltage, the EPD parameters were optimized (30 V), when the system was worked beginning the hydrogen and oxygen liberation at cathode electrode to continuous the coating process. The deposited samples were collected from the bath during the deposition process and dried overnight in an air atmosphere [9]. The pulses have a millisecond length, and the average current density is calculated:

$$Ia = Ip\ Ton/Ton + Toff = Ip\ Ton\ f = Ip*d \quad (1)$$

Where;

$$f = 1 / (Ton + Toff) \text{ and } d = Ton\ f \quad (2)$$

Where f denotes the pulse frequency and d denotes the duty duration, which is the proportion of a cycle that the current passes through the solution. Unless otherwise mentioned, deposition was carried out on pH 4.5 suspensions with a total pulse ON time of 30 seconds (Ton). It should be noted that as the pulse duration was decreased, the pulse width was reduced as well, Figure 2 depicts a standard current pulse wave, with clear square-wave bursts with desired duty cycles of 50 percent duty cycle [10]. A square wave is a form of pulse wave in which the positive and negative portions of the loop are equal; it is often known as a "50 percent duty cycle." It's called a pulse wave if the two halves aren't identical [11].

$$D = \mathit{T}on/(\mathit{T}on + \mathit{T}off) \quad (3)$$

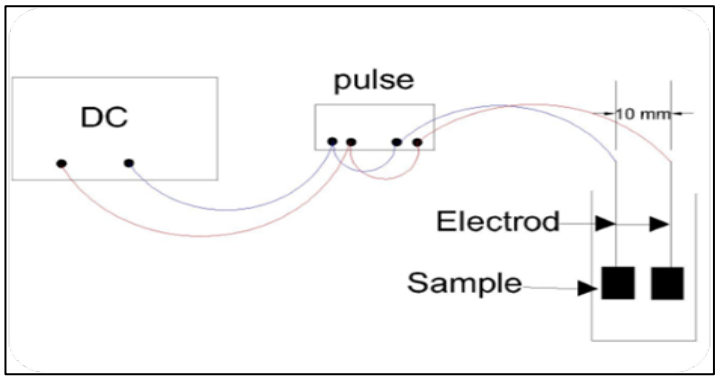

Figure 1: Pulsed Electrophoretic deposition setup

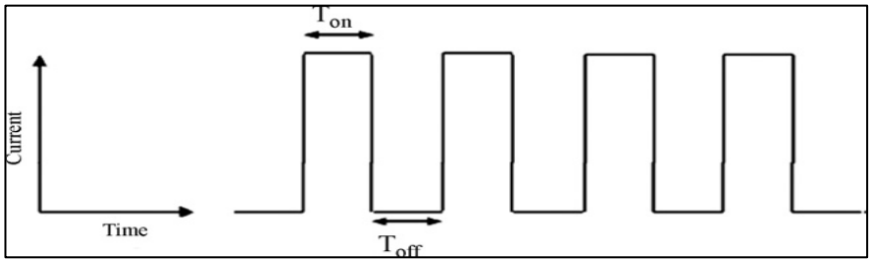

Figure 2: A standard current pulse with a service period of 50%

2.4 The samples

This research includes preparing 36 samples with dimensions (15*15*1) mm of 316L stainless steel and coating them with pulsed EPD HAp/CS composite coating layer at constant voltage (30 V) and frequency (50Hz), Table 1 explain the all-variables process.

Table 1: Variables of pulsed EPD process

	Group A (Freq.=50 Hz)			
	Samples	***Hap Co.***	***Time of Dep. T(min)***	***Duty %***
	S1	0.15	10	25
	S2	0.3	10	25
	S3	0.4	10	25
	S4	0.6	10	25
	S5	0.15	10	50
	S6	0.3	10	50
	S7	0.4	10	50
	S8	0.6	10	50
A1	S9	0.15	10	75
	S10	0.3	10	75
	S11	0.4	10	75
	S12	0.6	10	75
	S13	0.15	15	25
	S14	0.3	15	25
	S15	0.4	15	25
	S16	0.6	15	25
A2	S17	0.15	15	50
	S18	0.3	15	50
	S19	0.4	15	50
	S20	0.6	15	50
	S21	0.15	15	75
	S22	0.3	15	75
	S23	0.4	15	75
	S24	0.6	15	75
	S25	0.15	20	25
	S26	0.3	20	25
	S27	0.4	20	25
A3	S28	0.6	20	25
	S29	0.15	20	50
	S30	0.3	20	50
	S31	0.4	20	50
	S32	0.6	20	50
	S33	0.15	20	75
	S34	0.3	20	75
	S35	0.4	20	75
	S36	0.6	20	75

3. Characterizations of Samples

3.1 Fourier transforms infrared spectroscopy (FTIR)

Fourier transform infrared spectroscopy (FTIR) was used to characterize the film at a wave number of 4000-500 cm^{-1} by using (FTIR-TENSOR-27, Bruker, Japan made) [12-14].

3.2 Contact Angle

One of the most common methods for determining a surface's or material's wettability is to use contact angle. The analysis of how a liquid deposited on a concrete substrate stretches out, as well as the tendency of liquids to shape boundary surfaces

with solid states, is referred to as wetting. A hydrophilic surface has a low water touch angle (90 °), which is thought to aid in the attachment of nutrients and bone-forming cells

3.3 X-ray diffraction (XRD)

X-ray diffraction (XRD) was used to identify phases 316L SS and normal HAp powder using a (LabX XRD-6000, Shimadzu, Japan x-ray) with CuK radiation (=0.154 056 nm) and a scanning speed of 8 (deg min1) at voltage=40 kV and current=30 mA at voltage=40 kV and current=30 mA. The size of crystallites was determined using Scherrer's formula and the equation:

$$D=0.9\lambda/FWHM\cos\theta\ (nm) \quad (4)$$

where: D: The scale of the crystallite (nm). λ = wavelength of Cu K has a: (0.15406 nm).
The absolute width at half height of the diffraction peak is referred to as the FWHM (deg).
The angle **θ** of diffraction (o) [16].

3.4 Yield deposition measured

The response of each control factor at the assigned levels was investigated by measuring the deposition yield, as given in Equation:

$$\text{Yield deposition} = w2\text{-}w1 / A \quad (5)$$

Where; w2 = weight of the sample after coating, w1 = weight of the sample before the coating. A (surface area of the coating) =1.5*1.2 cm^2 [16].

3.5 Zeta potential

The stability of the suspensions and the homogeneity of the coatings were analyzed by zeta potential. This test was performed in Nano Technology Center, University of Technology. The four concentrations of hydroxpatite were examined [15].

This test was performed using Zeta plus (Brookhaven instrument Corporation, USA) in the Nanotechnology and Advanced Materials Research Center – University of Technology – Baghdad. The following steps were performed for setting up the samples for zeta potential:

1. Prepare the device for operating.
2. Ultrasonic treated of the suspension for 15 min before the test.
3. Add (1ml) of KCl to the suspension that to be examined.
4. Vibration the suspension completely.
5. Filtrate the suspension three times and then measurement.

3.6 Optical microscopy (OM)

Optical microscopy (OM) was used to detect the phases of the 316L S.S. The examination was using (optical microscopy, EMZ-DR MEIGI). It comprised of ocular lens, objectives lenses with three magnification power, light source, detector for light aggregation and camera connected with computer to show the metallographic pictures and the estimating of dimensions [17].

3.7 Field Emission Scanning Electron Microscope (FESEM) and Energy dispersive x-ray analysis (EDX)

Using a field emission scanning electron microscope, the surface morphology and transverse section of the deposited coatings layer were examined in Iran (MIRA3 RESCAN). Energy dispersive X-ray spectroscopy (EDX) coupled to the FE-SEM is used to examine the local elemental composition of the substrate and composite coatings.

4. Results and Discussions

4.1 Characterization of basic materials

4.1.1 FTIR Characterization of CS and HAp powders

From Figures below it is demonstrated that the infrared spectrum of chitosan and hydroxpatite powders, where the chemical structures are (C8H13O5N) n and Ca10 (PO4)6(OH) 2 respectively. The infrared spectrum of results from the group frequencies of the Phosphate bands, carbonate bands and Hydroxyl bands Figures 3.a, & 3.b show FTIR peaks of different bands appeared for the HAp Nano powder [12-14]. All FTIR results was explained in the Table2.

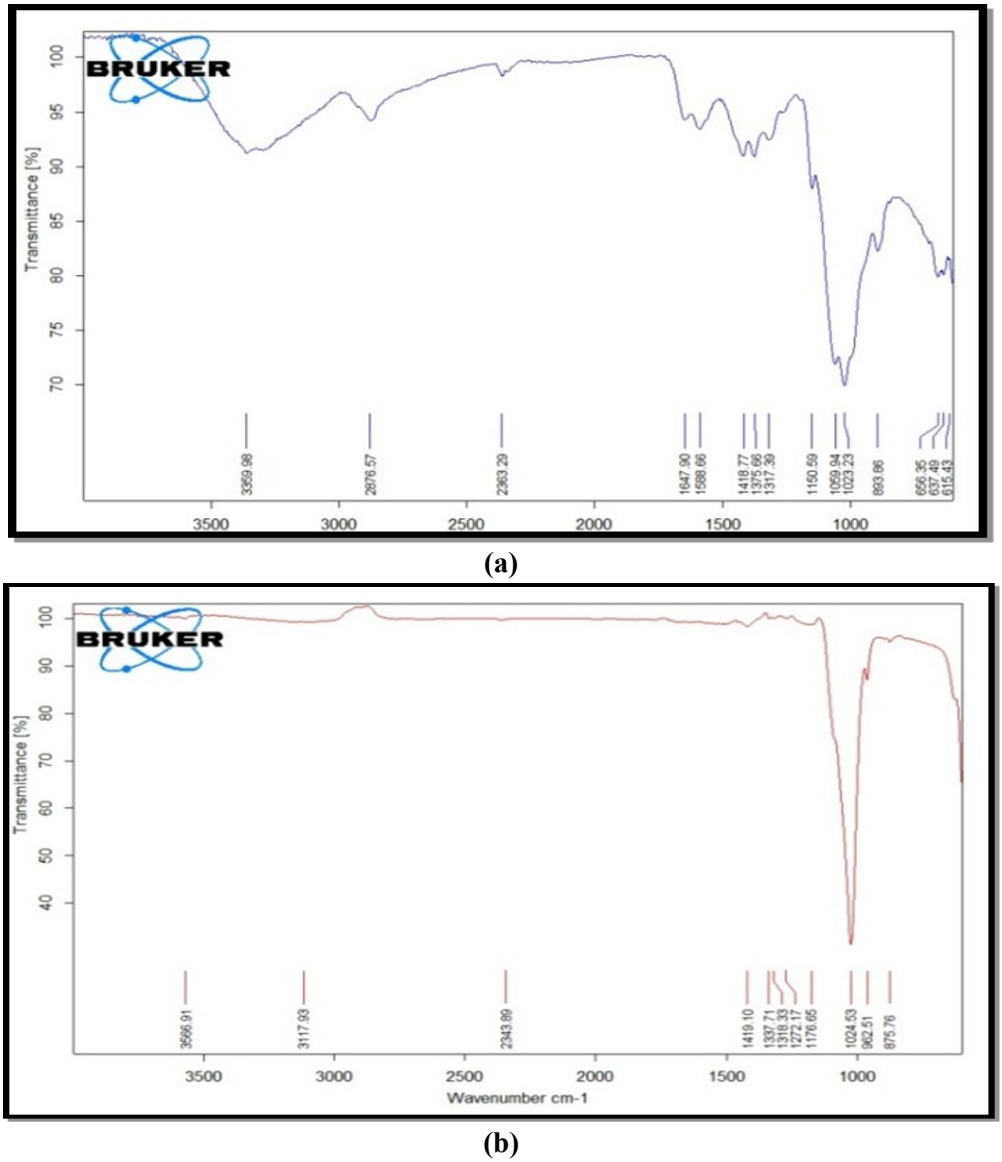

Figure 3: FTIR spectra of (a) CS powder, (b) standard Hap Nano- powder

Table 2: General band assignment, wave number and band modes FTIR spectrum analysis for CS and HAp powders

Wave number		**Band Mode**	
CS	***HAp***	***Phosphate bands***	
-	962	V1 (PO4)-3	symmetrical P-O stretching
1023, 1059	1024	V3 (PO4)-3	asymmetrical P-O stretching
615, 637	-	V4 (PO4)-3	O-P-O bending
Carbonate bands			
-	1419	V1 (CO3)-2	asymmetrical C-O stretching
893	875	V2 (CO3)-2	O-C-O bending
Hydroxyl bands			
1647	-	δ (OH)	O-H-O bending
1375,1317	1318,1337	C-C group	
1150	1176	C-N stretching	carbonate bond
-	1272	Complex vibration	NHCO3 group (amide 3 band)

4.1.2 XRD Characterization of HAp nano-powder

A Figure 4, shows the XRD patterns for the HAp powder at (002), (211), (300), (310) and (213) were the 2θ values for the HA peaks found to be at 25.9289° 32.0837°, 33.0398°, 40° and 49° which is assigned to (JCPDS 09-0432) for pure HAp. The broadening of XRD peaks is mainly attributed to the decrease in crystallite size indicating a nano-crystal line nature of the powder under investigation stoichiometric HA is stable over the neutral. The identification phases of HAp powder are measured before their deposition presents in Figure 4 and Figure 5. All diffraction lines were consistent with JCPDS file no. 9-432 for stoichiometric HAp.This indicates that no trace elements including ammonium, nitrate, Potassium, sodium and chloride ions that can be easily incorporated into the lattice structure led to nonstoichiometric HAp. It has been demonstrated that potassium (K^+) ions substituting calcium (Ca^{+2}) in the lattice structure of HAp while chloride (Cl^-) ions are found to

substitute hydroxyl (OH) groups and this leading to formation nonstoichiometric HAp in the bulk crystal [16]. Table 3 explain Crystallite size of highest three peeks for Nano HAp. Table 3 shows that the average crystallite size of regular HAp powder is about 16 nm. It shows that the HAp powder crystal Size used in this study is less than 20 nm in size.

In the Figure 6 reveals the XRD pattern and quantitative analysis of the sample S14(Conc. HAp 0.3g T15, min, D 25%, F 50 Hz). The XRD of the coating formed diffraction peaks that correspond to the JCPDS 09-432 hydroxyapatite standard card. The resultant peak broadening may be attributed to the coating material's small crystal dimension. The calculation was performed by using Scherrer equation and peak widths from X-ray diffraction. As a result of the coating material's limited crystal dimension, peak broadening occurred. Table 4 shows that the average crystallite size of the coated sample S14 is about 29nm. It shows the XRD study of the coated coating reveals a high degree of crystalline with little alteration in the crystal structure. Furthermore, due to the lack of contact between the coating particles at ambient temperature, no phase decomposition occurs during the EPD process.

Table 3: For regular HAp, the crystallite size of the top three peeks

peak	2θ (deg)	cos θ	FWHM (deg)	I	λ (A^O)	D=0.9λ/FWHM cos θ (nm)
1	32.0837	0.9610	1.091	100	1.5406	13.2
2	33.0398	0.9587	0.773	46	1.5406	18.7
3	25.9289	0.9745	0.762	31	1.5406	18.6

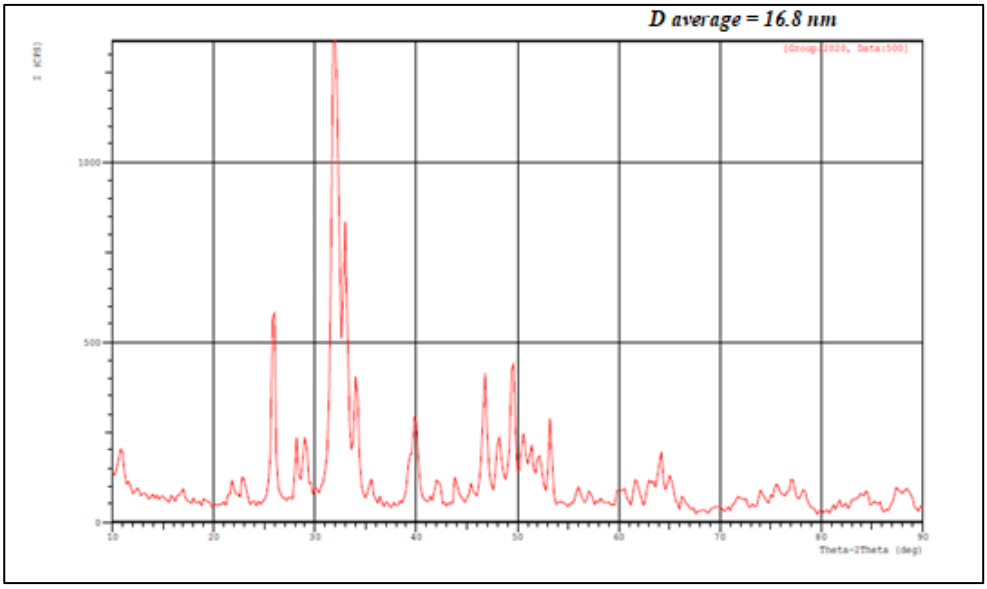

Figure 4: Diffraction pattern of HAp powder

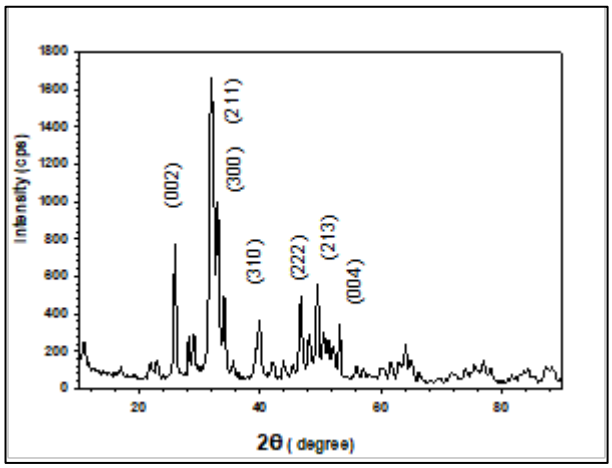

Figure 5: Diffraction pattern of HAp powder

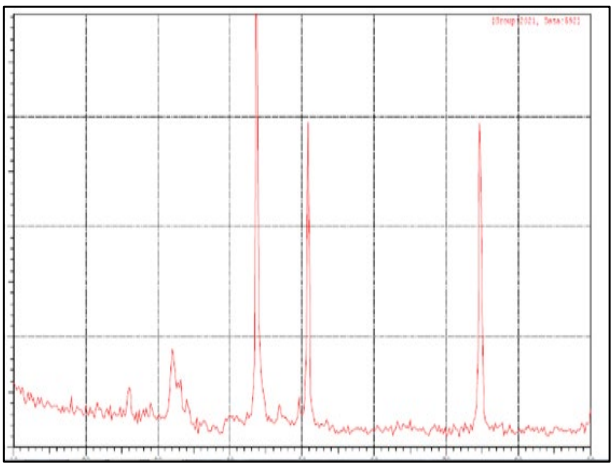

Figure 6: XRD: of sample S14(conc. HAp0.3g, T15 min, D 25%, F 50 Hz)

Table 4: XRD pattern of sample S14, the crystallite size of the top three peeks

peak	θ (deg)	cos θ	FWHM(deg)	I	λ (nm)	D=0.9λ/FWHM cos θ (nm)
1	43.7219	0.9280	0.54390	100	1.5406	27.4
2	74.6595	0.7952	0.53820	78	1.5406	32.3
3	50.8343	0.9032	0.50550	67	1.5406	29.43

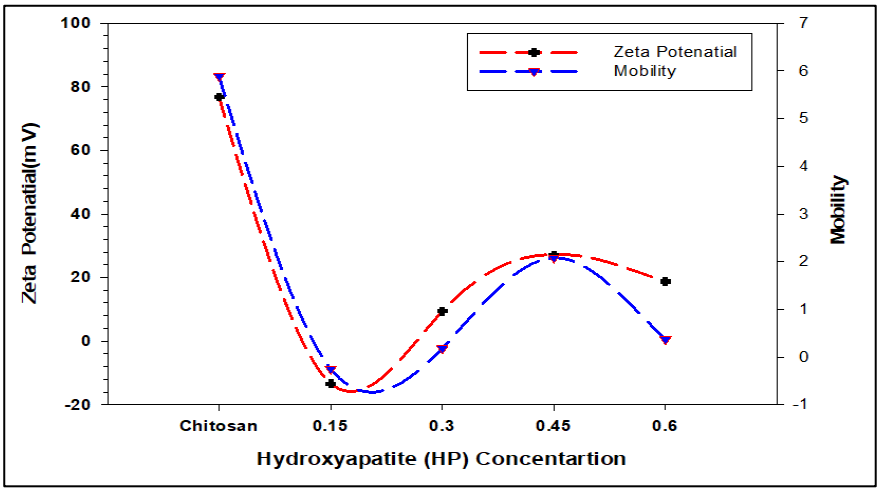

Figure 7: Zeta potentials of pure chitosan and chitosan/Hap nanoparticles in suspensions Containing (0.15, 0.3, 0.45, and 0.6) g/L

4.1.3 Zeta potentials Characterization for HAp/CS nano-composite suspensions.

The zeta potential was used to determine the stability of the suspension and the uniformity of the coating. To better understand the suspension stability and deposition mechanism, zeta potential measurements were taken. Suspensions containing pure CS and CS/HAp (0.3, 0.45 and 0.6) g/L HAp had zeta potentials of (76.78, 9.39, 27.13and 18.74) mV, respectively. Both suspensions' zeta potential values were found to be positive. This means that the HAp nanoparticles are catholically deposited. The CS/HAp composite with a concentration of (0.15) exhibits a negative value of (-13.43). In addition, the mobility of Suspensions containing pure CS and CS/HAp (0.3, 0.45, and 0.6) g/L HAp had values of (5.89, 0.18, 2.08, and 0.37) m^2/s. V, respectively, the zeta potential and mobility explain in Figure 7. The fact that the (CS with HAp) suspension has a higher potential than the CS suspension suggests that the Hap improves CS particle stability in the medium [15].

4.2 Characterization of coated samples

4.2.1 Yields determination of HAp/Cs coating layer on S316L by EPD

To obtain the w1, w1 by using a sensitive balance type calibrated with (± 0.0001% accuracy). The deposits were dried for 24 hours in the air and at room temperature; the weight gain was determined by comparing the weights of the substrates before and after deposition to calculate the weight of CS/HAp composition coatings. In this study, Group consisted of 36 samples were selected as below: Group A classified into (A1, A2, and A3) at a frequency of 50 Hz, as shown in Table 5 below. The yield was determined in terms of deposition time, the concentration of Nano-hydroxyapatite, and Duty cycle value in this study. The curves for the HAp/CS method are shown in Figures 8 (a, b, c) with a deposition time of 10,15 and 20 minutes and a steady current of 795 mA. Tables V display the deposit yield for Group A using a constant voltage catholic pulse EPD at 30V, frequency 50 Hz, with various HAp concentrations of (0.15, 0.3, 0.45, and 0.6) g and service cycles of (25 percent, 50 percent, and 75 percent) respectively. The amount of bubble incorporation in the deposit could be regulated by adjusting the service cycle of the applied pulse voltage or current. The deposition was important for an applied current below 1% duty cycle, but grew steadily between 25% and 75% duty cycle. The findings revealed that as the pulse size is reduced, the yield decreases, and the amount of bubble integration decreases when pulsed DC is used. Figure 8 depicted the deposition yield as a function of concentration and duty cycle, both of which varied linearly with variables. (D=75%) is superior to S16 (0.0008 g/cm^2) at (D=25%) with the same conditions (c=0.6, t=15 min) [16]. The deposition quality improved as the HAp concentration and service duration were increased. The value of yield deposition at S36 (0.0030g/cm^2) with time deposition (20 min) is higher than S24 (0.0021 g/cm^2) with time deposition (10 min) at the same concentration and duty cycle. Yield deposition of S28 (0.0012 g/cm^2) at (c =0.15) is greater than S25 (0.0006 g/cm^2) at (c=0.6) at the same conditions (D=25%, time =20 min). The magnitude of yield S20 (0.0017 g/cm^2).

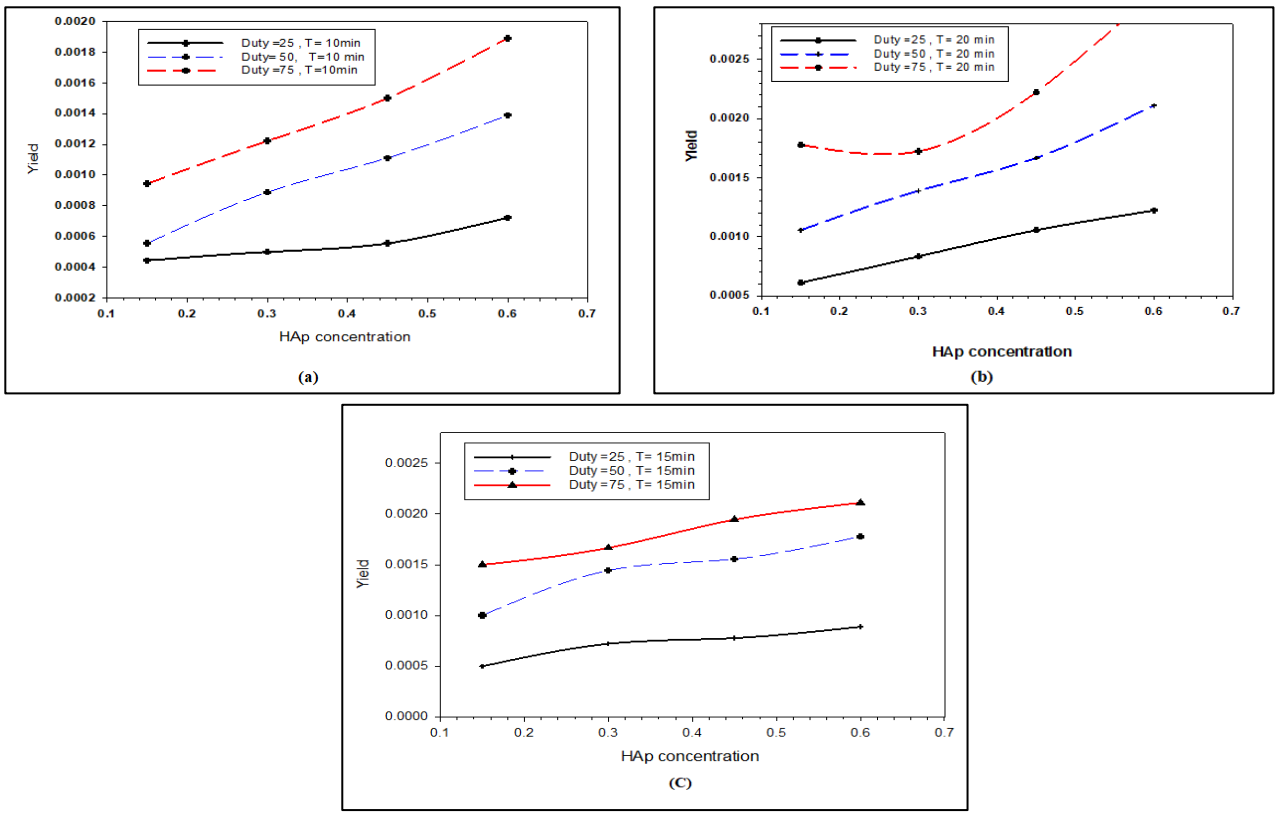

Figure 8: Yield with a deposition time of 10, 15, and 20 minute

Table 5: Variables of pulsed EPD process and yield magnitude.

	Group A (Freq.=50 Hz)				
	Samples	**Hap Co.**	**Time of Dep. T(min)**	**Duty%**	**Yield**
A1	S1	0.15	10	25	0.0004
	S2	0.3	10	25	0.0005
	S3	0.4	10	25	0.0005
	S4	0.6	10	25	0.0007
	S5	0.15	10	50	0.0005
	S6	0.3	10	50	0.0008
	S7	0.4	10	50	0.0011
	S8	0.6	10	50	0.0013
	S9	0.15	10	75	0.0009
	S10	0.3	10	75	0.0012
	S11	0.4	10	75	0.0015
	S12	0.6	10	75	0.0018
A2	S13	0.15	15	25	0.0005
	S14	0.3	15	25	0.0007
	S15	0.4	15	25	0.0007
	S16	0.6	15	25	0.0008
	S17	0.15	15	50	0.001
	S18	0.3	15	50	0.0014
	S19	0.4	15	50	0.0015
	S20	0.6	15	50	0.0017
	S21	0.15	15	75	0.0015
	S22	0.3	15	75	0.0016
	S23	0.4	15	75	0.0019
	S24	0.6	15	75	0.0021
A3	S25	0.15	20	25	0.0006
	S26	0.3	20	25	0.0008
	S27	0.4	20	25	0.0010
	S28	0.6	20	25	0.0012
	S29	0.15	20	50	0.0010
	S30	0.3	20	50	0.0013
	S31	0.4	20	50	0.0016
	S32	0.6	20	50	0.0021
	S33	0.15	20	75	0.0017
	S34	0.3	20	75	0.0017
	S35	0.4	20	75	0.0022
	S36	0.6	20	75	0.0030

4.2.2 Optical microscopy structural characterization HAp/Cs coating layer on S316L by EPD

Optical microscopy (OM) was used to detect the phases of the 316L SS. It comprised of the ocular lens, objectives lenses with three magnification power, light source, a detector for light aggregation, and camera connected with computer to show the metallographic pictures and the estimating of dimensions. Figure 9 (a, c, e) and (b, d, f) shows the surface optical microscopy of the samples coated at time (10, 15, and 20) min at HAp concentration of 0.15 and 0.6 g/L and the frequency value of 50 HZ respectively. The samples (a, c, e) showed a continuous, uniform, and crack-free HAp layer coating. Due to the high thickness (41 µm) and roughness =0.489 (Sa) (nm) of the coatings, pits, large porous, and grains can be seen on the surface of HAp samples (b, d, f). During EPD, pits and macro-porous regions form due to hydrogen evolution at the cathode, which increases coating porosity. Shrinkage and cracking of coatings may occur during heat exposure due to residential development as well as thermal stresses caused by differences in thermal expansion coefficients between the ceramic coating and the metallic substrate; cracking is more common for thick coatings. According to Wei et al. [18], the thermal expansion coefficient of 316L stainless steel (17.2 x 10^{-6}/°C) is 45 percent greater than that of HAp (9.9×10^{-6}/°C), so the stainless-steel layer must have placed the coating into substantial stress after increasing density to preventing coating cracks.

4.2.3 Contact Angle

The coating of (CS) leads to decrease the contact angle from 53.9±0.5° to 25.523º which in turn converted the uncoated surface of the 316L SS alloy from hydrophobic to hydrophilic. When the sample S22 (duty cycle 75%, time deposition =15 min and concentration of HAp=0.3g) was obtained the CS/HAp composite coating layer more hydrophilic have contact angle 20. 563º.The sample S31 at concentration 0.3 is hydrophilic have contact angle 20.843º converted to the more hydrophilic with increasing the concentration of HAp to (0.6 g) with contact angle 13.732º for the same time and duty cycle. In this case the bone regeneration will be easier and more rapt. When there are decreasing in contact angle with CS- HAp coating is deposited on substrate coating, The above description of the contact angle values for uncoated and coated 316L SS alloy are shown in the Figure 10. Water contact angles for samples are altered between 30.543º which considered as a hydrophilic to 13.732º which considered as super a hydrophilic. These results, by pulsed EPD were obtained super hydrophilic surfaces need in the medical applications [19].

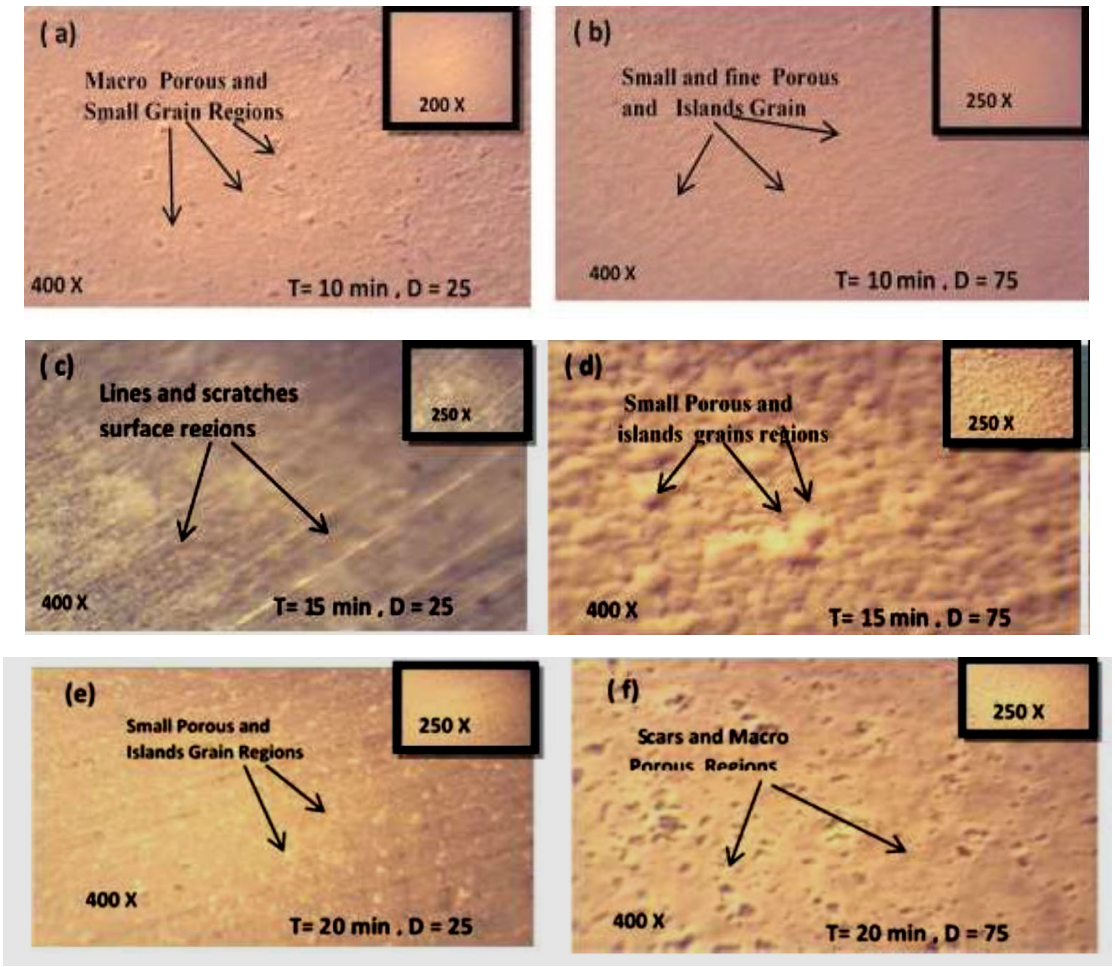

Figure 9: Optical image Microscopy of samples (a, c and e) at HAp concentration of 0.15 g/L. And (b, d and f) at HAp concentration of 0.6 g/L Within frequency value of 50 HZ

4.2.4 Field emission scanning electron microscopy (FE-SEM) and Energy Dispersive X-Ray Spectroscopy (EDX).

FE-SEM images used to demonstrate the surface morphology of HAp/CS composite coating layers that is obtained by Pulsed EPD technique on stainless steel 316L. In order to form suitable coatings, the influence EPD pulse current frequency (50 and 300) Hz on the surface morphology of the deposition layer of HAp /CS on S316L substrate was studied. In general, in the FE-SEM images the bright area represents the hydroxyapatite phase in matrix dark areas represent the (chitosan) phase. The FE-SEM images of the S316L substrate samples EPD coated (0.15HAp /CS) at deposition time (10 min) at frequency 50Hz is shown in Figure 11. The coating on the sample at 10 minutes (a) appeared smooth, uniform, and crack-free, compare with sample at high frequency for the same conditions shown in the Figure 8, due to the high frequency growing thickness and roughness of the coatings, cracks and pits can be seen on the surface of samples coated at 10 minutes. Pits form at high frequency and high HAp concentration (0.6g) in EPD are related to hydrogen evolution at the cathode, which increases coating porosity. As well as, the thermal stresses resulting from differences in thermal expansion coefficients between ceramic and metallic coatings can induce shrinkage and cracking of the coatings, which is more dominant for thick coatings [20, 21].

The elemental composition of the HAp/CS coating deposited on the 316L SS substrate for different pulsed EPD parameters. The elemental composition of the bioactive coating on the surface of the metallic implant is critical since it must correspond to the composition of the bone source. As it refers to the properties of calcium phosphate coatings used in biomedical applications, the (Ca/P) ratio is important. It's important to note that different bone structures have different ratios than that of the HAp theoretic, the atomic percentages of calcium (Ca) and phosphor (P), as well as the Ca/P ratio of the coatings of 0.15 HAp/CS (F 50 Hz, D 25%) is 2.05. This may be explained by the increases in the porosity of the coatings layer [20], shown in the Figure 12.

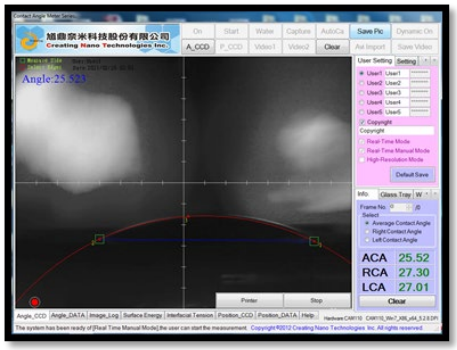

Θ=25.523º, sample coated with chitosan

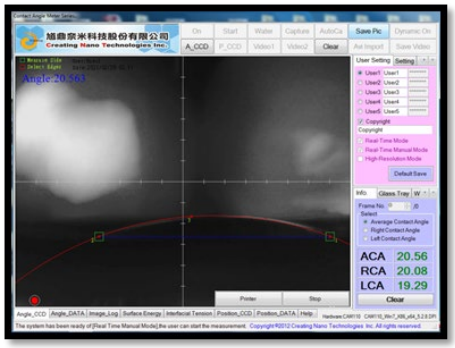

Θ=20.563º, S22

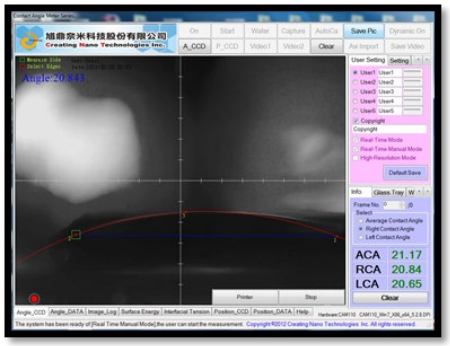

Θ=20. 843º, S31

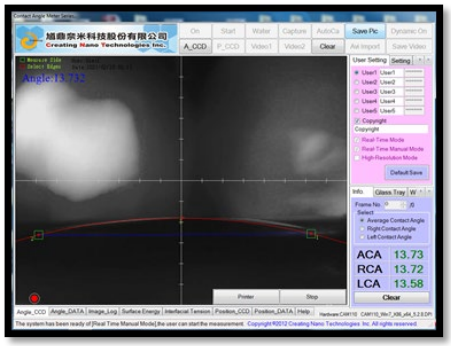

Θ=13,732º,S32

Figure 10: Photograph of Droplet Water of Stainless Steel (316L SS) Substrate with Coating

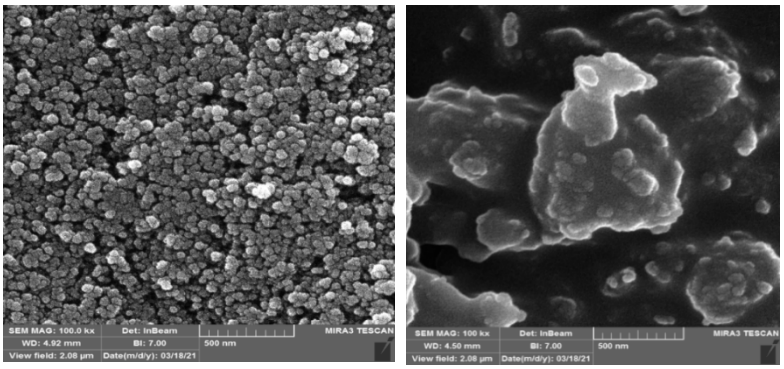

Figure 11: FE-SEM images of 0.6 HAp/CS on S316L:(a) 10min for at frequency 50 Hz, (b) 10 min at frequency 300 Hz

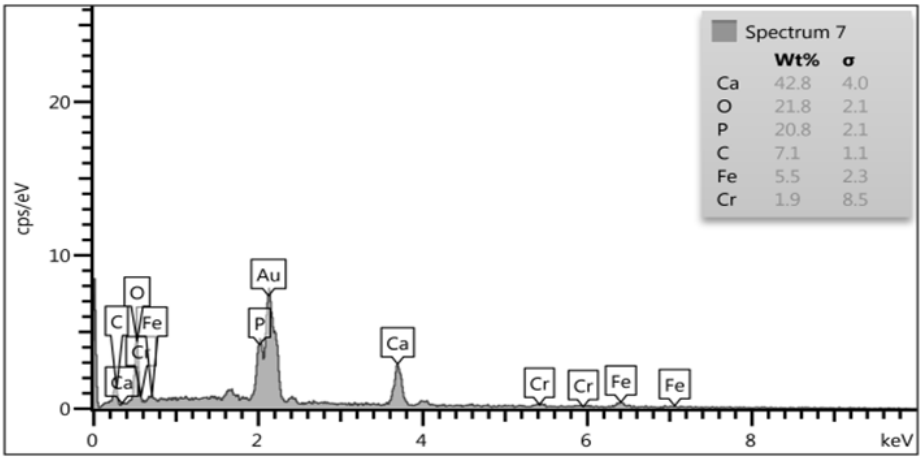

Figure 12: EDX images of 0.15 HAp/CS on S25 deposited at time 10min, F 50 Hz, D=25%

5. Conclusions

According to the results and findings, the following points are concluded: -

1. The addition of hydroxyapatite improved the stability of aqueous chitosan suspensions, allowing for pulsed electrophoretic deposition.
2. A suitable yield deposition on the 316L Stainless steel serving implant is led with hydroxyapatite concentration=0.6 and d=75 percent for suspension.
3. Optimal parameters were determined through a series of trial-and-error tests, the first of which was conducted on the 316 stainless steels. The "best" parameters were determined to be a voltage of 30 V, a HAp concentration of 6 g/L, a pH of 4.5, a deposition period of 20 minutes, and an inter-electrode distance of 10 mm.
4. The presence of peaks contributed to HAp, and chitosan in the coating isolated from the substrate was demonstrated by FTIR analysis
5. Pulsed current electrode position methods were used to successfully coat HAp on 316L SS without any post-treatment.
6. The pulse duty cycle can also be regulated depending on the OM image yield and bubble incorporation in the deposit. The lower the service cycle, the less bubble integration there was, and vice versa.
7. The truth is that the (HAp with CS) suspension has a higher - potential than the plain HAp suspension suggests that the CS improves HAp particle stability in the medium.
8. Yield deposition increased with increased deposition time.

Acknowledgment

The staff of Materials Engineering Department, University of Technology to characterization of the coated samples.

Author contribution

All authors contributed equally to this work.

Funding

This research received no specific grant from any funding agency in the public, commercial, or not-for-profit sectors.

Data availability statement

The data that support the findings of this study are available on request from the corresponding author.

Conflicts of interest

The authors declare that there is no conflict of interest.

References

[1] M. Niinomi, M. Nakai and J. Hieda, Development of new metallic alloys for biomedical applications, Acta Biomater., 8 (2012) 3888–3903. https://doi.org/10.1016/j.actbio.2012.06.037

[2] H. A. Zaman, S. Sharif, M. H. Idris and A. Kamarudin, Metallic biomaterials for medical implant applications: A Review, Applied Mechanics and Materials, 735 (2015) 19-25. https://doi.org/10.4028/www.scientific.net/AMM.735.19

[3] D. Sivaraj, K. Vijayalakshmi,Enhanced antibacterial and corrosion resistance properties of Ag substituted hydroxyapatite/functionalized multiwall carbon nanotube Nano composite coating on 316L stainless steel for biomedical application, Ultrasonic – Zoochemistry, 636 (2019). https://doi.org/10.1016/j.ultsonch.2019.104730

[4] I. V. Antoniac, Handbook of bioceramics and biocomposites, Springer, 1st ed., UK, (2016).

[5] I. A. Deen, Electrodeposition of organic inorganic films for biomedical applications, MSc. thesis, McMaster University, Canada, 9, (2012).

[6] E. Avcua, F.E. Baştanb, H. Z. Abdullahb, M. A. Rehmanb, Y.Y Avcub, A.R. Boccaccinib , Electrophoretic deposition of chitosan-based composite coatings for biomedical applications: A review, Prog. Mater Sci.,103(2019). https://doi.org/10.1016/j.pmatsci.2019.01.001

[7] L. C. Arias, S. C. Polo, H. Gao, J. Gilabert, E. Sanchez, J. A. Roether, D. W. SchubertS, Virtanen and A. R. Boccaccini, Electrophoretic deposition of nanostructured-TiO2/ chitosan composite coatings on stainless steel, RSC Advances, 28 (2013) 11247-11254. https://doi.org/10.1039/C3RA40535D

[8] F. Pishbin, A. Simchi, M.P. Ryan and A.R. Boccaccini, Electrophoretic deposition of chitosan/45S5 Bio-glass composite coatings for orthopedic applications, Surf. Coat. Technol., 205 (2011) 5260–5268. https://doi.org/10.1016/j.surfcoat.2011.05.026

[9] Z. M. Al-Rashidya, M.M. Faragb, N.A. Abdel Ghanyc, A.M. Ibrahimd, W. I. Abdel-Fattaha Orthopedic bioactive glass/chitosan composites coated 316L stainless steel by green electrophoretic co-deposition, Surf. Coat. Technol., 334 (2018). https://doi.org/10.1016/j.surfcoat.2017.11.052

[10] S.K. Ghosha, A.K. Grovera, G.K. Deyb, M.K. Totlania, Nano-crystalline Ni-Cu alloy plating by pulse electrolysis, Surf. Coat. Technol. , 126(2000) 48-63. https://doi.org/10.1016/S0257-8972(00)00520-X

[11] L. Besra, U. Tetsuo, T. S. Suzuki, Y. Sakka, Experimental verification of pH localization mechanism of particle consolidation at the electrode/solution interface and its application to pulsed DC electrophoretic deposition (EPD) , J. Eur. Ceram. Soc., 30 (2010) 1187-1193. https://doi.org/10.1016/j.jeurceramsoc.2009.07.004

[12] D. Nú ñez, E. Elgueta, K. Varaprasad and P. Oyarzún, Hydroxyapatite nanocrystals synthesized from calcium rich bio-wastes, Mater. Lett., 230 (2018) 64-68. https://doi.org/10.1016/j.matlet.2018.07.077

[13] D. He, P. Wang, P. Liu, X. Liu, F. CangMa and J. Zhao, HA coating fabricated by electrochemical deposition on modified Ti6Al4V alloy, Surf. Coat. Technol., 301(2016) 6–12. https://doi.org/10.1016/j.surfcoat.2016.07.005

[14] A. Teymouri, B. J. Stuart and S. Kumar, Hydroxyapatite and dittmarite precipitation from algae hydro lysateAlgal Res., 29 (2018) 202–211. https://doi.org/10.1016/j.algal.2017.11.030

[15] T. A. Salah, A. M. Mohammad, M. A. Hassan, B. E. El-Anadouli, Development of nano-hydroxyapatite/chitosan composite for cadmium ions removal in wastewater treatment, J. Taiwan Inst. Chem. Eng., 45 (2014) 1571-1577. https://doi.org/10.1016/j.jtice.2013.10.008

[16] M. A. Rehman, M. A. Munawar, D. W. Schubert, A. R. Boccaccini, Electrophoretic deposition of chitosan/gelatin/bioactive glass composite coatings on 316L stainless steel: A design of experiment study, Surf. Coat. Technol., 358 (2019) 976-986. https://doi.org/10.1016/j.surfcoat.2018.12.013

[17] M. J. Kadhim, N. E. Abdulateef, M. H. Abdulkareem, Evaluation of surface roughness of 316L stainless steel substrate on nano hydroxyapatite by electrophoretic deposition, Al-Nahrain J. Eng. Sci., 21 (2018) 28-35. https://doi.org/10.29194/NJES21010028

[18] A. D. Hikmawati, P. Widiyanti, T. Amrillah, A.Nia, I. T. Firdania and C. A. Abdullah, Study of mechanical and thermal properties in nano-hydroxyapatite/chitosan/carboxymethyl cellulose nano composite-based scaffold for bone tissue engineering: the roles of carboxymethyl cellulose, Appl. Sci., 19 (2020) .https://doi.org/10.3390/app10196970

[19] B. M. Marzec, D. R. Wielgus, M. B.´Nski, B. Bartosewicz and A. Z. nski, Comparison of properties of the hybrid and bilayer MWCNTs—hydroxyapatite coatings on Ti Alloy, Coatings, 9 (2019) 643. https://doi.org/10.3390/coatings9100643

[20] D. Gopi, J. Indira, L. Kavitha, A comparative study on the direct and pulsed current electrode position of hydroxyapatite coatings on surgical grade stainless steel, Surf. Coat. Technol., 206 (2020) 2859-2869. https://doi.org/10.1016/j.surfcoat.2011.12.011

[21] L. Sorkhi, M. F. Rad, T. Shahrabi, Electrophoretic deposition of hydroxyapatite– chitosan–titania on stainless steel 316 Surfaces, Surface, 2 (2019) 458-467. https://doi.org/10.3390/surfaces2030034